

Multiscale modeling of island nucleation and growth during Cu(100) homoepitaxyM. Basham,¹ F. Montalenti,² and P. A. Mulheran^{1,*}¹*Department of Physics, University of Reading, Whiteknights, Reading RG6 6AF, United Kingdom*²*INFN and L-NESS, Dipartimento di Scienza dei Materiali della Università degli Studi di Milano-Bicocca, Via Cozzi 53, I-20125 Milano, Italy*

(Received 6 September 2005; published 19 January 2006)

The long-time scale dynamics of small Cu/Cu(100) islands are studied. Atomistic simulations using embedded atom method (EAM) potentials and the dimer method saddle point searches provide pathways and their temperature-dependent rates to lattice-based kinetic Monte Carlo (KMC) simulations. The KMC utilizes translational symmetry to identify previously visited sites and re-use the atomistic rates. As a result very long time scales are accessible to the simulation which reveals the dissociation as well as the diffusion mechanisms of the small islands in an unbiased manner. Our results for island diffusion reproduce well the activation energies calculated in previous work, and provide in addition the associated frequency prefactors. The island dissociation pathways are rationalized in terms of previously anticipated mechanisms. We also utilize our results in mean field rate equations to predict “kinetic phase diagrams” for the critical island size as a function of temperature and vapor deposition rate during Cu(100) homoepitaxy. We predict that the higher critical island sizes ($i > 2$) should be observable at higher temperatures (above ~ 500 K) at experimentally accessible deposition rates.

DOI: [10.1103/PhysRevB.73.045422](https://doi.org/10.1103/PhysRevB.73.045422)

PACS number(s): 68.35.Fx, 82.20.Wt

I. INTRODUCTION

Island nucleation and growth during thin film deposition has received a lot of attention in recent years from modelers, theorists, and experimentalists alike.¹ Simple metal homoepitaxy such as Cu/Cu(100) growth is particularly appealing since it is amenable to scanning tunneling microscopy imaging² as well as detailed atomistic modeling using embedded atom method potentials. The challenge for modelers is the time scale spanned by the growth process. The material is usually deposited from vapor at rates of one monolayer per second or slower, allowing the adatoms to diffuse long distances after deposition before becoming incorporated into islands or nucleating new ones. Traditional molecular dynamics simulations of adatom kinetics, which access the nanosecond time scale, are almost completely ineffectual in providing deep understanding of the growth process. Modelers and theorists have, therefore, turned to a number of alternative techniques to address key questions of interest.

One common modeling technique uses lattice-based Monte Carlo, where a set of simplified simulation rules is specified in advance.³ These rules usually allow for the random deposition of monomers onto the lattice at a rate of F monolayers per second (ML/s), coupled with adatom random walks on the lattice with diffusion constant D_1 .^{4–8} The evolution of the simulation is governed by the ratio of these rates; typically $R = D_1/F \approx 10^5 - 10^{10}$. The simulations also allow for island nucleation when the critical island size i is exceeded at a site on the lattice. The islands may be kept as single points regardless of size, or they can have footprints on the lattice that grow as they absorb impinging monomers. Islands are usually assumed to be immobile, although some studies where they diffuse with size-dependent rates have been performed.^{9–11} It is apparent that most of these lattice-based simulations do not attempt to achieve atomistic real-

ism, but rather they are “coarse-grained” in that they only incorporate processes that impact overall film morphology such as island sizes and their spatial arrangements. In this sense the models are very successful in reproducing salient features observed experimentally, and it is particularly noteworthy that scale-invariant properties of island arrays discovered in these simulations inspired further theoretical and experimental studies.^{12–15}

Another highly successful approach, first employed before modern computer power made simulation so accessible, is to model the nucleation and growth of islands through a set of reaction-diffusion rate equations.¹⁶ The hierarchy of equations for each size of island are usually solved in a mean-field limit where the islands are all assumed to sample the same environments and thus be exposed to the same monomer concentrations. Once again this approach has achieved noteworthy success for predicting island densities and average size as a function of substrate coverage at various values of the ratio R . Variations on the approach include solving for the island capture rates in a self-consistent manner,¹⁷ and allowing for island mobility and coalescence.¹⁸ The approach has also spawned theoretical analyses for the scaling properties of the rate equations, and good agreement with the lattice-based Monte Carlo simulations mentioned above has been achieved. The inability of this approach to successfully model island size distributions has also inspired further theoretical work, notably through the “capture zone” concept which goes beyond the mean field approximation.^{8,12–14}

Recent developments in addressing long-time scale events in atomistic simulations have started to make it possible to consider the atomistic detail of island nucleation and growth processes. Voter has developed “hyperdynamics” and “temperature accelerated dynamics” techniques which allow molecular dynamics simulations to find pathways from one configuration to the next at accelerated rates, so that realistic

simulations for island diffusion can be achieved.¹⁹ Henkelmann and Johnsson have developed the “dimer method” for finding saddle points in the 3N-dimensional space of a N-atom cluster, and this can be used to power “self-learning” kinetic Monte Carlo (KMC) simulations where the rules for the state-to-state transitions do not have to be pre-determined.^{20,21} Both these approaches mean that atomistic detail can be modeled for small-island mobility, and both reveal that diffusion mechanisms can involve multi-atom cooperative motions, mechanisms that might never have been considered in the original lattice-based Monte Carlo approaches. In particular the self-learning KMC technique of Henkelmann and Johnsson provides a versatile methodology highly suited to the study of island nucleation and growth and we exploit their approach in this work. We also note that very recently Trushin *et al.*³⁰ have similarly exploited the possibility of reaching extended time scales by using self-learning KMC techniques in a study of island diffusion on Cu(111).

Here we use a combination of the above methodologies (atomistic and dimer method-based KMC simulations, rate equations and scaling analysis) to produce a multiscale model of island nucleation and growth during Cu(100) homoepitaxy. Our motivations are the following. Experimentally we can hope to observe the island density and size distribution at various stages of the film growth; How do these properties depend on the atomistic details of the island dynamics? In general high critical island size i is preferable because it yields narrower size distributions and better spatial organization, and this in turn will influence the regularity of complete films and multilayer growth. But what influence do temperature and deposition rate have on i ? It is usually assumed that high temperature means high i because small clusters can then break apart more easily, based on simple nearest-neighbor bond-counting rules,^{22,23} but can this be quantified? Low deposition rate F also might yield high values of i through “slow” island dissociation events occurring before new material arrives,²⁴ or alternatively through the diffusion of small islands leading to coalescence with larger islands.²⁵ In the future we might also want to predict the impact various surfactants have on the film morphology, and again knowledge of atomistic processes must be scaled up to reveal their overall morphological consequences.

In this paper we start from the atomistic modeling of island mobility and stability, use the results in mean field rate equations of island nucleation and growth, and finally analyze its island density data in terms of the scaling theory growth exponents to create “kinetic phase diagrams” of i at various temperatures and deposition rates. The modeling can be said to be truly multiscale, passing from atomic detail through to the morphological properties of the evolving submonolayer film. In the next section we describe our self-learning KMC simulations and present the results for small island diffusion mechanisms and rates including activation energies and frequency prefactors. We also present results for island dissociation mechanisms and their associated energies and prefactors. In Sec. III we present details of the rate equations and the results they produce using our island mobility and dissociation data. In Sec. IV we apply a scaling analysis of the rate equations to our data to create the kinetic phase

diagrams. Finally in Sec. V we discuss the various results of this work.

II. ATOMISTIC MODELING OF ISLAND MOBILITY AND DISSOCIATION

A. Self-learning kinetic Monte Carlo simulation

In this work we investigate the dynamics of small Cu/Cu(100) islands using an optimized EAM potential that reproduces well *ab initio* values for single adatom hop and exchange activation energies.^{26–28} The island dynamics are explored using the dimer method to discover pathways from the current configuration to new potential minima separated by one saddle point. The harmonic approximation to transition state theory yields the temperature-dependent rates of the possible transitions, and these rates are then used in a kinetic Monte Carlo simulation.

The strategy of the simulation is illustrated in Fig. 1 We start with a small island on top of a bulk-termination (100) surface. In the KMC representation [Fig. 1(a)] the island is a “lattice animal” centred at the origin of a square lattice. The island also has an atomistic representation, Fig. 1(b). The atomistic simulation will be used to discover the transitions available to the island, and their associated temperature-dependent rates. This data is fed back to the KMC simulation, which then selects what transition to make and increases the simulation clock according to the usual algorithm.²⁹ The original lattice animal is now updated to the new state [see Fig. 1(a)], which is re-centered while a record is kept of the center-of-mass displacement of the island. If the updated lattice animal is new to the simulation, then it is passed to the atomistic simulation to initiate a new batch of saddle point searches. However, if the lattice animal has been visited before, the transition pathways out of the configuration have already been discovered and so the KMC can proceed immediately. We note that this strategy is similar in spirit to the one recently used to study Cu/Cu(111) island diffusion and coalescence.³⁰

The atomistic simulation cell has periodic boundary conditions parallel to the free surface. The bottom few layers of the cell are fixed in their bulk positions, and the top 3 layers plus the atoms in the island are all allowed to move in the saddle point searches. The dimer method works by exploring the 3N-dimensional configuration space, starting from random atomic displacements within the current potential well. A dimer is created from two images of the system displaced by a small fixed separation from one another. The dimer is then moved according to a simple manipulation of the forces on each image, forcing it to climb the potential surface in the direction of lowest curvature until a saddle point is reached. Many separate searches are initiated from different starting points in the current potential well, in order to get a thorough sampling of the available transition pathways. In addition, to test the completeness of the sampling, a single high-temperature ($T=700$ K) basin-constrained molecular dynamics simulation is run up to the first attempted transition. If this transition has not been discovered in the Dimer searches, more of the latter need to be started. Once the pathways and their associated rates have been calculated from the activa-

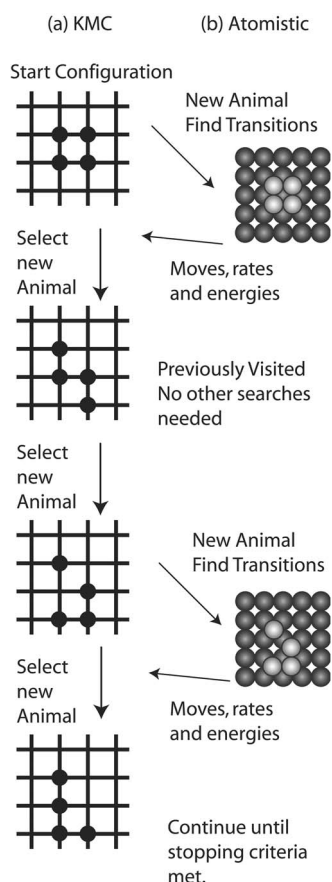


FIG. 1. Diagrammatic representation of the self-learning KMC simulation. The KMC uses lattice “animals” [column (a)] to represent the island configuration. New configurations are passed to the atomistic simulation illustrated in column (b). The atomistic simulation performs dimer method saddle point searches to find possible pathways out of the current configuration, along with their associated activation energies and frequency prefactors. This “event list” is returned to the KMC which selects the next configuration and increments the simulation clock as usual. If the new configuration has been visited before, then no new searches need be initiated in the atomistic simulation.

tion energy and Vineyard prefactors, the data is passed back to the KMC.

The advantage of this combined atomistic-KMC simulation is that the transition pathways are not restricted to single atom motions but can include multi-atom shears, etc.²¹ The methodology also ensures that the saddle-point data from each configuration only has to be discovered once. The KMC itself is a very rapid simulation, whereas the saddle point searches each can take about 250 force evaluations in the atomistic simulation, and this can be quite cpu-intensive for the larger islands. The moves most commonly selected by the KMC simulation at low temperatures are often the lowest energy ones that usually do not contribute to the overall diffusion of the islands or indeed to their fragmentation. The lattice-animal KMC can run through millions of these fast events per second. The events of most interest to us are the higher energy ones that cause significant center-of-mass motions, and which leave the island in less compact configura-

tions where exposed atoms can break away to cause the island to dissociate. Indeed, in the simulations presented here each run continues until the island has dissociated.

It is worth commenting at this stage that the simulation methodology is quite versatile. The lattice animals are constructed from the adatoms on top of the surface, and can include any vacancies in the surface layer. However, in the simulations we have performed, the high-activation energy event of vacancy-adatom pair creation is never selected by the KMC. Although events do occur by the exchange of adatoms with surface atoms, this is naturally accommodated by the way the lattice animals are identified.

Before we present our results for the mobility and stability of the small islands, we remark on a limitation of the simulation. The dimer method is not guaranteed to find all the transitions that are available to the system, and so a large number of searches are required to try to ensure that the lowest energy ones have been found.³¹ In Fig. 2(a) we show the center-of-mass movements of a four-atom (tetramer) island at 500 K, where 50 saddle point searches are used for each lattice animal in the KMC. After 5600 iterations the movement looks like an acceptable random walk. However, in Fig. 2(b) we show the movements over millions of iterations, during which time the island has not yet dissociated, and we clearly do not have a random walk. The bias in the island’s motion arises from not discovering all the accessible transition pathways. If we increase the number of dimer searches for each lattice animal to 250, we do obtain a random walk over the time scales of interest [Fig. 2(c)].

B. Results for small island diffusion

We have run the self-learning KMC simulations for adatom islands of sizes 1–8 at a range of temperatures 400–900 K. Each simulation was run until the island dissociates, and 1000 runs for each size and temperature combination were used to obtain reliable statistics. The diffusion constant for each island is obtained from its center-of-mass motion in the simulations, and in Fig. 3(a) we show that the data follow the Arrhenius law for temperature dependence. In Fig. 4(c) we show the activation energies and in Fig. 4(b) the frequency pre-factors for the islands’ hopping rates. It is interesting to note how the energy for diffusion does not monotonically increase with size at these small sizes, but oscillates as predicted in other studies. An interesting effect here is that the dimer movement has lower activation energy than the single monomer diffusion. This may be an artifact of the potential being used, although other studies in this area (including *ab initio* calculations) seem to confirm this result.^{32,33}

Figure 4(c) also shows the results for the activation energy for island diffusion found by Trushin *et al.*,^{32,33} calculated from the presumed rate-limiting move for each island. Our results are in close agreement with theirs, and the key atomistic moves that cause the island diffusion are the same as we discovered in our self-learning simulations. In one sense our work provides independent confirmation of the earlier study, but it has done this without prejudice for the moves the simulation is likely to select. A more detailed

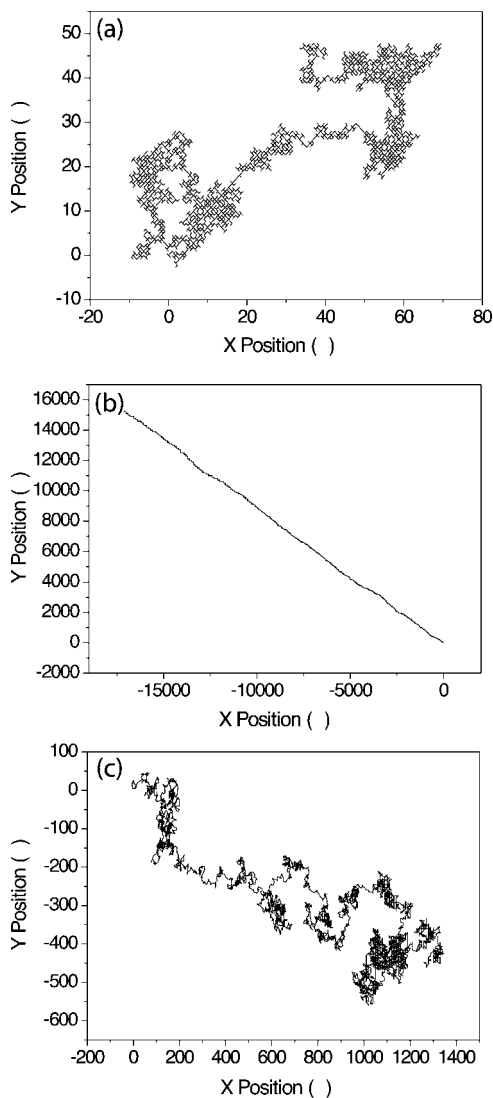


FIG. 2. Results for the center-of-mass movement of a tetramer island at 500 K. In (a) and (b) only 50 dimer method searches were used for each configuration visited; (a) shows 5600 steps whereas (b) shows several million steps. In (c) several million steps are shown using 250 saddle point searches for each configuration.

comparison with Refs. 32 and 33 for the atomistic mechanisms and rates for island diffusion will be presented in a future work.

An advantage that our simulation enjoys is that it provides the frequency pre-factors in an unbiased way, relying only on the Vineyard pre-factors for individual atomic motions (including substrate atoms). Note in Fig. 4 how the variation of frequency pre-factors with size follows the trend of the activation energy, with large frequency accompanying large energy. This feature has been observed before in Ref. 31 where multi-atom movements tended to have high frequency pre-factors.

Finally in Fig. 4(a) we also show the temperature at which an island will be stationary for 1 s, which is a time scale relevant to many homoepitaxy experiments. It is noteworthy that islands of size 4, 6, and 8 are stationary on these time scales at higher temperatures (270 K) than the other islands

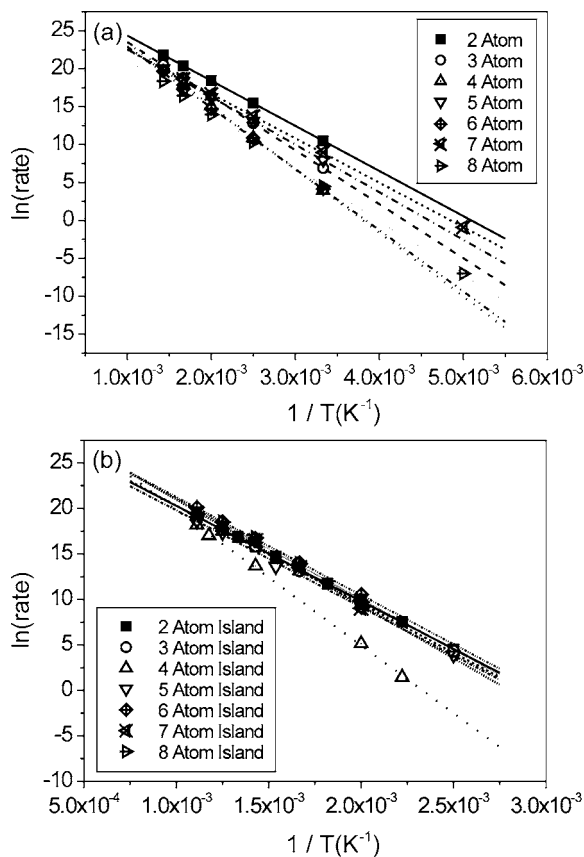


FIG. 3. Arrhenius plots for the dynamics of islands of various size: (a) Shows center-of-mass hopping rates, and (b) shows island dissociation rates.

(200 K). This will impact the kinetics of island nucleation and growth which we will consider below.

C. Results for small island dissociation

We turn our attention now to the island dissociation events and their temperature-dependent rates. In Fig. 3(b) we show that the dissociation data nicely obey the Arrhenius Law expected for thermally activated processes. We shall present a little more detail about the dissociation pathways.

Figure 5 shows the main dissociative pathways for the three-atom (trimer) island, showing a sequence of island configurations, their associated energies, and the saddle-point energy for the transitions between one state and the next (the energies shown are relative to the most stable island configuration). The dissociation pathways are quite diverse, and range from the dimer walking away from the adatom to the adatom hopping away from the dimer. However, the processes all present the same total activation energy barrier.

For larger size islands, the most probable dissociation events are dominated by two types of pathways, both of which involve a single atom moving away from an island edge. In essence the atom which is likely to dissociate from the island needs to be in a situation with one nearest-neighbor (NN) and one next-NN (NNN) in-plane atom. One way of the dissociation move occurring is with a single hop directly away from the island, with an approximate activa-

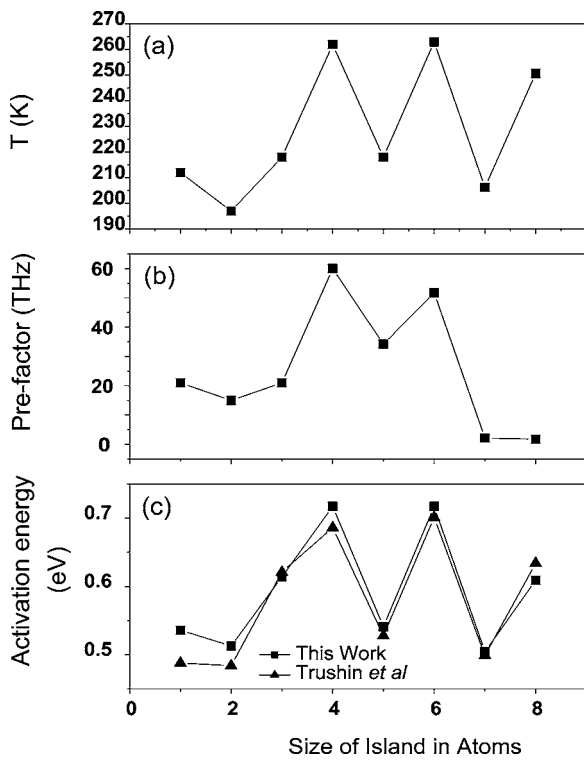


FIG. 4. Island mobility results from this work. In (a) we show the temperature at which the island will remain stationary for 1 s (on average). In (b) and (c) we show the frequency prefactors and the activation energies, respectively, for island hopping.

tion energy of ~ 0.9 eV, as illustrated in Fig. 6(c) for the tetramer island. The second more elaborate move is two separate transitions: The first is “sideways” away from the NN so it becomes a NNN, a move of approximately 0.6 eV, then a following move of ~ 0.5 eV which takes the atom away from the island, as illustrated in Fig. 6(a). Again the interesting point about the second of these pathways is that the total energy barrier that needs to be overcome is the same as in the first direct pathway, with a net activation energy of ~ 0.9 eV. This means that both events have equal likelihood of occurring and are, therefore, both very valid paths for dissociation.

The mechanisms described above for this type of dissociation are valid for all sizes of island. This does not mean, however, that all sizes of island dissociate with the same energy, as the island has to get into an appropriate state (where at least one atom has only one in-plane NN) before it can dissociate. This is obviously very easy for the trimer or five-atom island, as it is automatically in the appropriate position in its minimum energy configuration. The four- or nine-atom islands though are much harder to dissociate, as they have to break their minimum energy configuration to get into a situation close to where the dissociation event might occur.

The above discussion indicates that the dissociation energy might be found by considering the reverse process, whereby a single adatom hops back into an island in its final post-dissociation configuration, and subsequently the recombined island relaxes to its most stable configuration

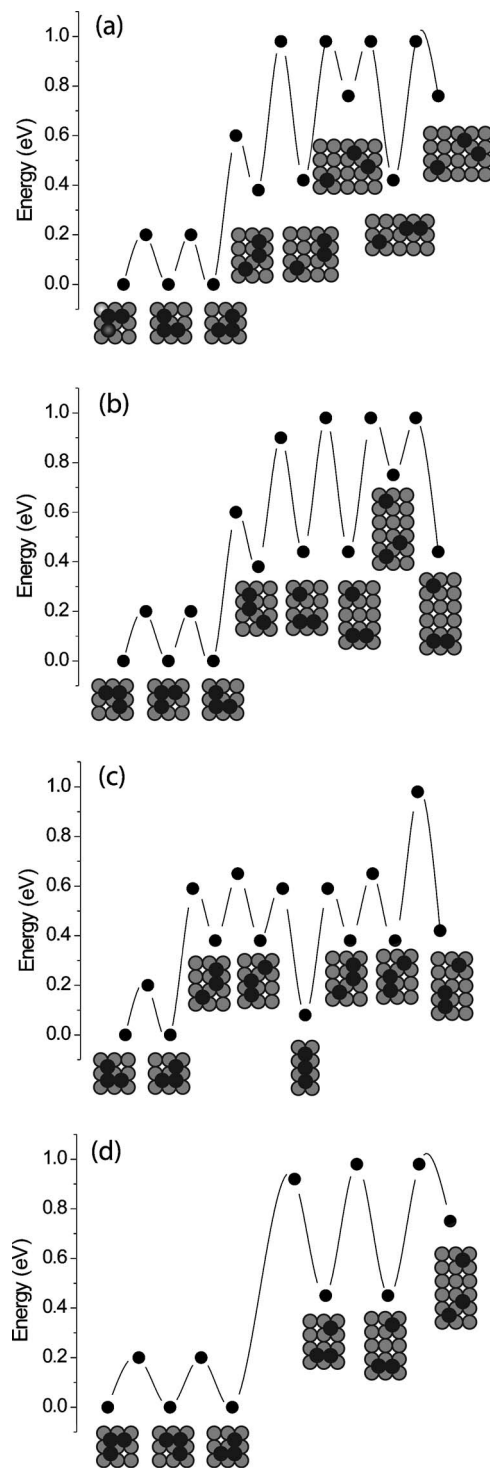


FIG. 5. The main dissociation pathways for a trimer island discovered in our self-learning KMC simulations.

[view the sequence of states in Fig. 6(c) from right-to-left].³⁴ The height of the energy barrier from the initial configuration through to the dissociated state is then

$$\Delta E = E_f - E_i + \Delta E_h, \quad (1)$$

where E_f and E_i are the energies of the final and initial configurations, and ΔE_h is the activation energy of the single adatom hop.

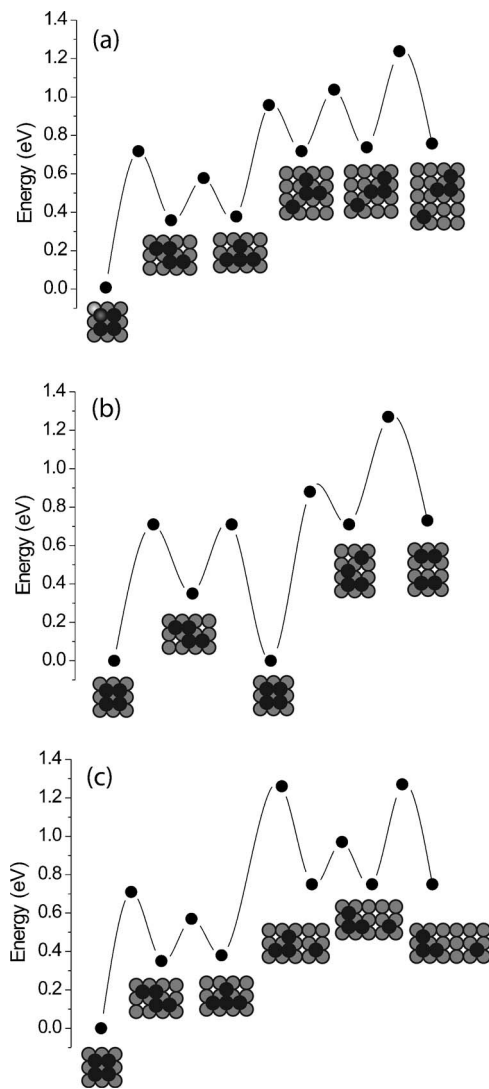


FIG. 6. Some dissociation pathways for a tetramer island discovered in our self-learning KMC simulations.

Equation (1) does give a good result for the smaller islands, although it yields no indication of the frequency prefactor. This method, however, does not appear to give an accurate representation of the activation energies for larger island dissociation. When the dissociation of the nine-atom island was studied, the simulation proved too time-consuming with our resources. We, therefore, used Eq. (1) to try to estimate the dissociation energy. However, the value that we obtained, which was in the region of 1.35 eV, was lower than the 1.8 eV event observed in the KMC simulation for a corner rounding event on the nine-atom island. If the simulation selects such a high energy process, it is extremely unlikely that a much lower energy dissociation event would not occur. Thus while this dissociation energy barrier may be plausible it certainly requires further investigation.

As a final point of interest on the dissociation pathways, there are also alternative dissociation pathways for smaller islands that may only have slightly higher activation energy. In Fig. 6(b) we show a dissociation pathway of the tetramer island which fragments it into two dimer islands with activa-

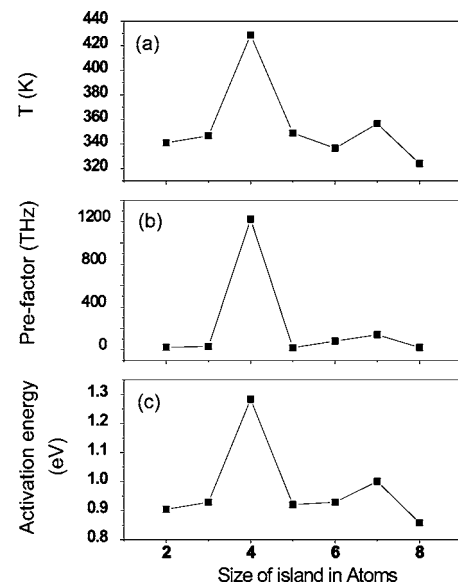


FIG. 7. Results for the island dissociation mechanisms discovered in the self-learning KMC simulation. In (a) we show the temperature at which islands are stable for 1 s (on average). In (b) and (c) we show the frequency prefactors and the activation energies, respectively, for island dissociation.

tion energy close to the single atom release move. This is of special interest, and although may be an event that occurs only infrequently in our simulations of Cu/Cu(100) island dynamics, may be much more prevalent when dealing with softer metals such as silver and aluminum.

In Fig. 7(c) we show the activation energies and in Fig. 7(b) the frequency prefactors for island dissociation taken from the Arrhenius plots of Fig. 3(b). The main point to note is the stability against dissociation of the tetramer island, which arises from the necessary shearing of the island before the single atom can break free from the edge (see Fig. 6, and Refs. 32, 33, and 35). A similarly high activation energy is anticipated for the nine-atom island although this remains to be confirmed in the self-learning KMC. The other small islands all dissociate at about the same energy. Note again that the frequency prefactors follow the trends of the activation energies, so that high energy events also have higher prefactors. We can combine the results to give in Fig. 7(a) the temperatures below which the islands are stable for at least one second (a characteristic time scale for homoepitaxy), which again highlights the stability of the tetramer island. Note in particular that as the temperature increases, the “critical island size” is not expected to show a steady increase, but might be anticipated to jump in value to $i=3$ at 340 K or so, and might increase again to $i=8$ at about 440 K. However, island diffusion will blur the boundaries and increase these “kinetic transition temperatures” as we see below.

III. RATE EQUATION MODELING OF ISLAND NUCLEATION AND GROWTH DURING HOMOEPITAXY

A. Mean field rate equations

In this approach, the evolution of the density of islands of various sizes is modeled through a hierarchy of rate equations:³⁶

$$\frac{dN_1}{dt} = F - D_1 N_1 \sum_{q=1} \sigma_q N_q (1 + \delta_{1q}) + \sum_{q=2} \kappa_q N_q (1 + \delta_{2q})$$

$$\frac{dN_s}{dt} = \sum_{q=1}^{q=s-1} D_q N_q \sigma_{s-q} N_{s-q} - D_s N_s \sum_{q=1} \sigma_q N_q - \sigma_s N_s \sum_{q=1} D_q N_q + \kappa_{s+1} N_{s+1} - \kappa_s N_s \quad (2)$$

where N_s is the density of islands of size s , D_s is the diffusion constant and κ_s is the dissociation rate of an island of size s , σ_s is its capture kernel, t is time, and F is the deposition rate. Islands of size $s \geq 10$ are combined together in a single class. These equations are mean field in that we assume that all islands of a given size capture material at the same rate, and fluctuations in their environments are neglected. We have also assumed that the dominant dissociation pathway of the islands is to release a single adatom.

In order to solve these equations numerically, we must specify the capture kernels. There are a range of possibilities to choose from with varying degrees of sophistication, however, for the purposes of this study we shall follow Kyuno *et al.*³⁶ and utilize the simplest choice:

$$\sigma_s = \begin{cases} 3, & s \leq 7 \\ 7, & s \geq 8. \end{cases} \quad (3)$$

This approximation is justified for small island capture, and we shall assume that islands of size nine atoms and above are perfectly stable and immobile. Equations (2) and (3) above are solved numerically using the temperature dependent dissociation and diffusion rates determined in the previous section. We employ a fourth-order Runge-Kutta scheme, starting with zero island densities.

B. Results

The clearest way to show the difference that the diffusion and dissociation of small islands make to the nucleation and growth dynamics is to compare the solutions to Eqs. (2) and (3) with various terms excluded. The following examples are, therefore, split into three different categories. All the simulations have monomer deposition and diffusion and this is used as a base-line comparison. The second solution allows small island diffusion, and the third allows both small island diffusion and dissociation.

Figure 8 shows the variation of island densities at 10% substrate coverage as a function of inverse temperature, where the deposition rate $F = 5 \times 10^{-3}$ monolayers per second. In Fig. 8(a), only monomer diffusion is allowed. The results are quite straightforward, as the densities of all the different sized clusters are approximately the same for most temperatures above 250 K. It is important to point out the fact that the density scale is logarithmic, and so the densities may be subtly different but all of the same order of magnitude. The main curve of interest is the density of the islands above 10 atoms, as these are the most likely to be seen easily in experimental situations. With this simulation the 10+ island density show a distinctive single gradient for $T > \sim 270$ K.

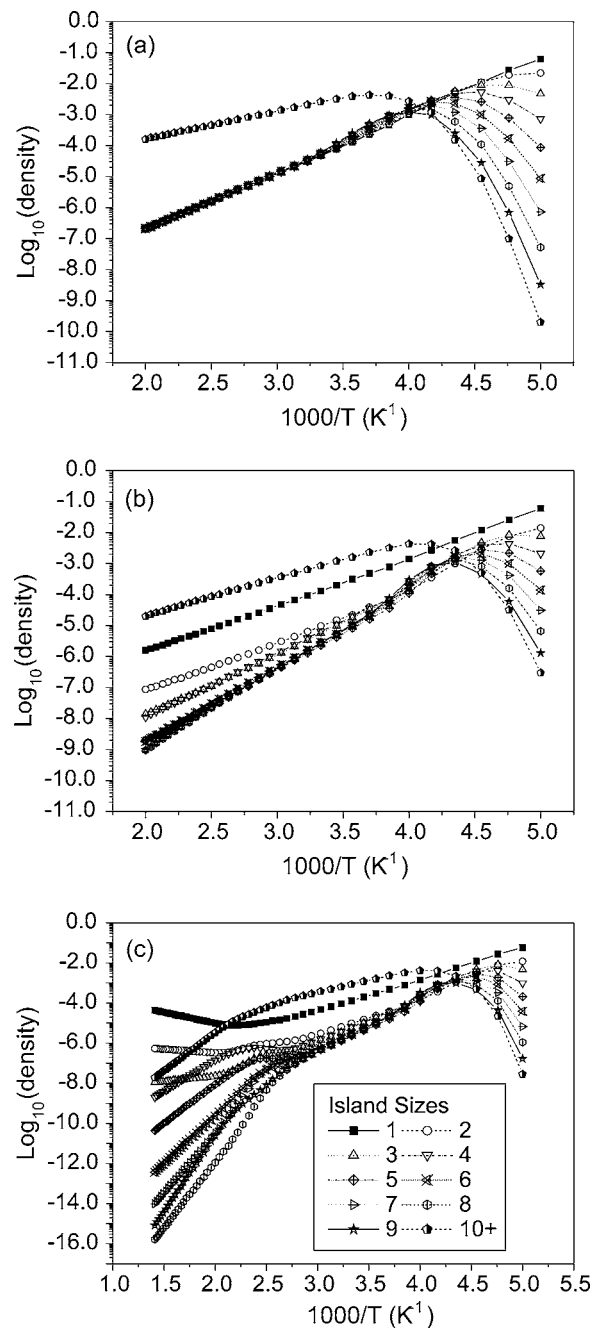


FIG. 8. Results from the mean field rate equations for the island densities vs temperature, taken at 10% substrate coverage with $F = 0.005$ ML/s. In (a) only monomers are mobile and all islands are stable; in (b) islands sizes 2–8 can also diffuse; and in (c) islands sizes 2–8 can dissociate and diffuse.

When all the islands are allowed to diffuse at their appropriate rates the results change significantly, as can be seen in Fig. 8(b). In this case the densities of different island sizes have different gradients, since they become mobile at different temperatures. One thing to notice is that the gradient for all the islands above 10 atoms in size is a little steeper than that in Fig. 8(a). The point at which it peaks also occurs at a slightly lower temperature.

In the next set of rate equations, we keep the island diffusion and also allow the islands to dissociate. This provides

a more dramatic change to the density curves as seen in Fig. 8(c). There is now a peak in the density of tetramer islands at about 400 K, due to its significant stability compared to the island sizes above it. When the system reaches 400 K all the islands of sizes 5–8 are prone to dissociate, so they can cascade down in size until they become tetramers, thereby increasing the tetramer density. Of course when the system is hotter than 400 K, the tetramer starts to dissociate as well, meaning that all islands of size 2–8 are able to dissociate readily and cascade all the way down to monomers. As a consequence, at low temperature the gradient for the monomers is similar to all the other clusters, as in Fig. 8(a). As the temperature exceeds about 350 K the gradient shallows, as this is when the various islands start to dissociate but with the tetramer island stable. At about 400 K the tetramer starts to dissociate as well, and this allows for an increased production of monomers, causing the monomer density to increase as temperature rises.

IV. KINETIC PHASE DIAGRAMS

In scaling theories of island nucleation and growth it is convenient to analyze the evolution of the island density in terms of a single parameter, the critical island size i , defined as the cluster size above which islands are stable. With this definition, Blackman *et al.* predicted that island density N varies as a simple power of $R=D_1/F$, the ratio of the monomer diffusion constant and the deposition rate:

$$N \sim R^{-\chi}, \quad (4)$$

where the growth exponent

$$\chi = \frac{i}{i+2} \quad (5)$$

for compact two-dimensional islands.³⁷

We analyze the results of the rate equations in the previous section to deduce the effective island size. In Fig. 9 the total island density at 10% substrate coverage is plotted for three temperatures as a function of deposition rate. The gradients of the double-logarithmic plots reveal χ and i through Eqs. (4) and (5). In Fig. 9(a) only monomer diffusion is allowed, and we find $i=1$ as we would expect unless the deposition rate is high compared to the monomer diffusion rate. In Fig. 9(b) we allow the diffusion and dissociation processes to occur. Note now the curvature in the higher temperature curves, indicating that the effective critical island size increases as the deposition rate goes down. This happens because some small islands are able to dissociate or diffuse and coalesce with others before new monomers attach to them. The overall island density is decreased by these processes and the effective critical island size increases.

Based on this style of plot in Fig. 9, we create “kinetic phase diagrams” in Fig. 10 which show the regimes of the different values of i deduced at different temperature and deposition rate. The gradients are taken locally from the curves in Fig. 9(b). We can imagine this happening in an experimental study where the data is unlikely to cover such a broad range of deposition rates, masking the curvature in the log-log plots.

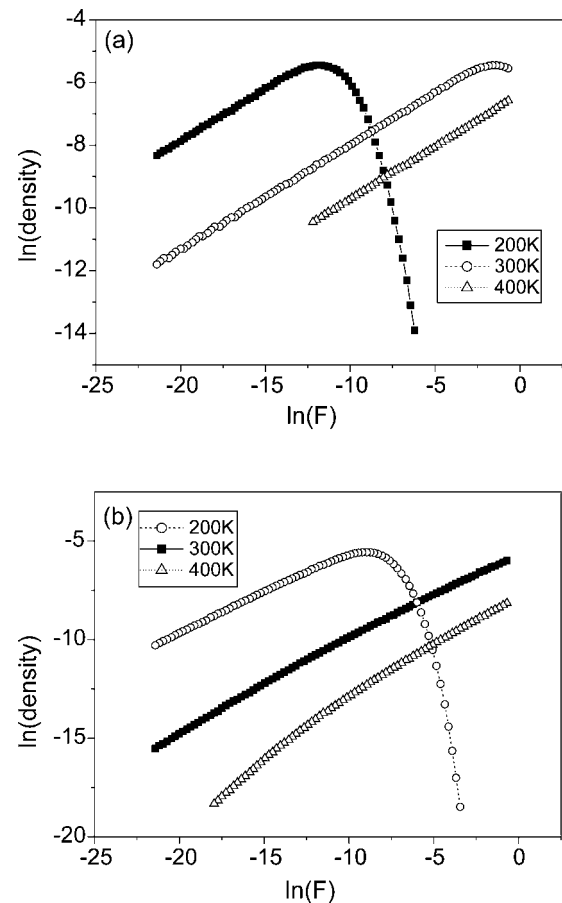


FIG. 9. Results from the mean field rate equations for the total island density vs deposition rate, taken at 10% substrate coverage. In (a) only monomers are mobile and all islands are stable; in (b) island sizes 2–8 can dissociate and diffuse.

Figure 10(a) shows the diagram when only the monomers are mobile. The diagram is simple to understand, since at low temperature the monomers are essentially immobile on the time scale of the film growth determined by the deposition rate. Hence at low temperature we classify the growth as $i=0$, since islands of size 1 are essentially stable.

Figure 10(b) shows our results when small island diffusion is included in the rate equations. We find a new domain of $i=2$, caused by the fact that the activation energy for dimer diffusion is lower than for monomer diffusion. As a consequence, the $i=1$ domain is of rather limited extent, existing around room temperature but not much higher than 400 K.

Finally in Fig. 10(c) we show the results for the analysis of the rate equation data when island dissociation and diffusion is allowed. Now we see that the $i=2$ domain only exists up to a certain threshold temperature, above which island dissociation starts to dominate the critical island size. The biggest surprise though is that one might have expected to see a strong regime of $i=3$ behavior due to the enhanced stability of the tetramer island. However, this is not case because of the curvature in the plots of Fig. 9(b) where the mixture of mobility and dissociation blurs the validity of the simplified scaling analysis of the rate equations.

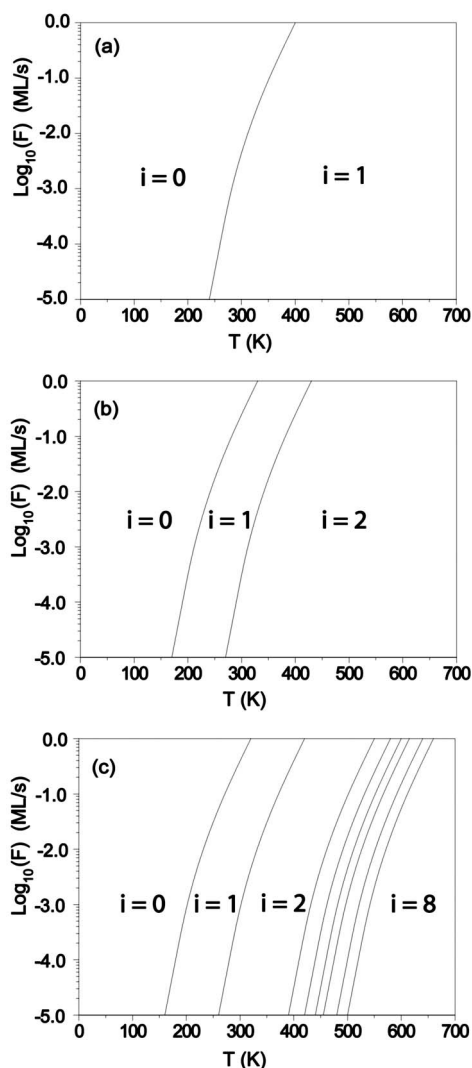


FIG. 10. Kinetic phase diagrams showing regimes of critical island size predicted by this work. In (a) only monomers are mobile and all islands are stable; in (b) islands sizes 2–8 can also diffuse; and in (c) islands sizes 2–8 can dissociate and diffuse.

V. SUMMARY AND DISCUSSION

We have presented results of a multiscale modeling of Cu(100) homoepitaxy. The atomistic part of the study used the recently proposed self-learning KMC approach powered by dimer method saddle-point searches^{20,21}. In order to simulate the evolution of the small Cu/Cu(100) islands up to their dissociation, we have employed a lattice representation of the atomistic configurations so that previous kinetic information can be re-used in the simulations. The atomistic model yields activation energies and frequency prefactors for island diffusion and dissociation rates, as well as providing insight

into the small island dissociation pathways. These parameters were then employed in mean field rate equations for island density dependence on temperature and deposition rate, which is summarized in the “kinetic phase diagrams” of the critical island size utilized in scaling theory.

Previous work on the multi-atom mechanisms of island mobility have emphasized the importance of the “dimer-shearing” movement illustrated in the first part of Figs. 6(a)–6(c).³⁵ Swan *et al.*²⁴ predicted that this mechanism leads to the fragmentation of islands size $s=4$, which our work has confirmed. However, they deduce a high critical island size from their low energy electron diffraction (LEED) data at the modest temperature of 213 K, at low deposition flux of $F \leq 10^{-2}$ monolayers per minute. Our work here shows no indication of this result; high critical island sizes only become apparent at much higher temperature in Fig. 10(c). However, in subsequent work the same team with Furman *et al.*³⁸ conclude that the experiments on the average inter-island separation were taken at too high substrate coverage (30%) where coalescence effects which are not included in the scaling theory may have started to dominate. They also performed Monte Carlo simulations to obtain good agreement with experiment at these coverages, and when analyzing the simulations at lower coverage they conclude $i=1$ at low temperature with an increase to $i=2$ (due mainly to dimer-island mobility) at 263 K. This is in much better agreement with our results. Furthermore, our work suggests re-visiting the Cu(100) homo-epitaxy experiments at higher temperatures to test the validity of Fig. 10(c).

The primary conclusion from this work is that we have demonstrated the feasibility of starting from atomistic models and working up to mesoscale morphological properties of the deposited sub-monolayer film. The atomistic modeling work is as thorough as we could make it with our existing computational resources, relying only on the validity of transition state theory and the efficacy of the EAM potentials. For the higher scale modeling, there are a number of more sophisticated options available for both the rate equations and the scaling analysis, however, it remains to be seen whether more work is justified here. The ultimate test of the results will be a thorough comparison with experiment, which we hope will happen in the future.

In conclusion we have shown how multiscale models of epitaxy can be constructed from the bottom up. Future models might look at other materials and surfaces, and include the role of surfactants.³⁹

ACKNOWLEDGMENT

This work has been supported by the UK’s Engineering and Physical Sciences Research Council through Grant Nos. GR/S25364/01 and GR/T18738/01.

*Corresponding author. Email address:

p.a.mulheran@reading.ac.uk

- ¹M. Zinke-Allmang, *Thin Solid Films* **346**, 1 (1999).
- ²W. W. Pai, A. K. Swan, Z. Zhang, and J. F. Wendelken, *Phys. Rev. Lett.* **79**, 3210 (1997).
- ³A. -L. Barabasi and H. E. Stanley, in *Fractal concepts in surface growth* (Cambridge University Press, 1995).
- ⁴P. Jensen, A. L. Barabasi, H. Larralde, S. Havlin, and H. E. Stanley, *Phys. Rev. B* **50**, 15316 (1994).
- ⁵M. C. Bartelt and J. W. Evans, *Phys. Rev. B* **46**, 12675 (1992).
- ⁶J. G. Amar, F. Family, and P. -M. Lam, *Phys. Rev. B* **50**, 8781 (1994).
- ⁷C. Ratsch, A. Zangwill, P. Šmilauer, and D. D. Vvedensky, *Phys. Rev. Lett.* **72**, 3194 (1994).
- ⁸P. A. Mulheran and J. A. Blackman, *Phys. Rev. B* **53**, 10261 (1996).
- ⁹P. A. Mulheran and D. A. Robbie, *Phys. Rev. B* **64**, 5402 (2001).
- ¹⁰L. Kuipers and R. E. Palmer, *Phys. Rev. B* **53**, R7646 (1996).
- ¹¹P. Jensen, A. -L. Barabasi, H. Larralde, S. Havlin, and H. E. Stanley, *Phys. Rev. B* **50**, 15316 (1994).
- ¹²P. A. Mulheran and D. A. Robbie, *Europhys. Lett.* **49**, 617 (2000).
- ¹³P. A. Mulheran, *Europhys. Lett.* **65**, 379 (2004).
- ¹⁴J. W. Evans and M. C. Bartelt, *Phys. Rev. B* **63**, 235408 (2001).
- ¹⁵J. G. Amar, M. N. Popescu, and F. Family, *Phys. Rev. Lett.* **86**, 3092 (2001).
- ¹⁶J. A. Venables, *Philos. Mag.* **27**, 697 (1973).
- ¹⁷G. S. Bales and D. C. Chrzan, *Phys. Rev. B* **50**, 6057 (1994).
- ¹⁸V. I. Trofimov and V. A. Osadchenko, *Growth and morphology of thin films* (in Russian, Energoatomizdat, Moscow, 1993).
- ¹⁹A. F. Voter, F. Montalenti, and T. C. Germann, *Annu. Rev. Mater. Res.* **32**, 321 (2002).
- ²⁰G. Henkelman and H. Jónsson, *J. Chem. Phys.* **111**, 7010 (1999).
- ²¹G. Henkelman and H. Jónsson, *Phys. Rev. Lett.* **90**, 116101 (2003).
- ²²J. G. Amar and F. Family, *Phys. Rev. Lett.* **74**, 2066 (1995).
- ²³J. A. Stroschio and D. T. Pierce, *Phys. Rev. B* **49**, R8522 (1994).
- ²⁴A. K. Swan, Z. -P. Shi, J. F. Wendelken, and Z. Zhang, *Surf. Sci.* **391**, L1205 (1997).
- ²⁵P. L. Krapivsky, J. F. F. Mendes, and S. Redner, *Phys. Rev. B* **59**, 15950 (1999).
- ²⁶A. F. Voter, *Phys. Rev. B* **57**, 013985 (1998).
- ²⁷A. F. Voter and S. P. Chen, in *Characterization of Defects in Materials*, edited by R. W. Siegel, J. R. Weertman, and R. Sinclair, MRS Symposia Proceedings No. 82 (Materials Research Society, Pittsburgh, 1987).
- ²⁸M. Basham, P. A. Mulheran, and F. Montalenti, *Surf. Sci.* **565**, 289 (2004).
- ²⁹A. F. Voter, *Phys. Rev. B* **34**, 6819 (1986).
- ³⁰O. Trushin, A. Karim, A. Kara, and T. S. Rahman, *Phys. Rev. B* **72**, 115401 (2005).
- ³¹F. Montalenti, *Surf. Sci.* **543**, 141 (2003).
- ³²O. S. Trushin, P. Salo, and T. Ala-Nissila, *Phys. Rev. B* **62**, 1611 (2000).
- ³³P. Salo, J. Hirvonen, I. T. Koponen, O. S. Trushin, J. Heinonen, and T. Ala-Nissila, *Phys. Rev. B* **64**, 161405(R) (2001).
- ³⁴Gerard Barkema (private communication).
- ³⁵Z. -P. Shi, Z. Zhang, A. K. Swan, and J. F. Wendelken, *Phys. Rev. Lett.* **76**, 4927 (1996).
- ³⁶K. Kyuno and G. Ehrlich, *Phys. Rev. Lett.* **84**, 2658 (2000).
- ³⁷J. A. Blackman and P. A. Mulheran, *Electronic, Optoelectronic and Magnetic Thin Films*, edited by J. M. Marshall, N. Kirov, and A. Vavrek (Research Studies Press Ltd., Taunton, U.K., 1995), p. 227.
- ³⁸I. Furman, O. Biham, J. -K. Zuo, A. K. Swan, and J. F. Wendelken, *Phys. Rev. B* **62**, R10649 (2000).
- ³⁹J. Camarero, J. Ferron, V. Cros, L. Gomez, A. L. V. de Parga, J. M. Gallego, J. E. Prieto, J. J. de Miguel, and R. Miranda, *Phys. Rev. Lett.* **81**, 850 (1998).